Renewable Energy 216 (2023) 119074

Contents lists available at ScienceDirect

Renewable Energy

journal homepage: www.elsevier.com/locate/renene

Variable period sequence control strategy for an off-grid photovoltaic-PEM electrolyzer hydrogen generation system

Xianyang Liu [a], Jun Zou [a,b], Rui Long [a,*], Zhichun Liu [a,**], Wei Liu [a]

[a] School of Energy and Power Engineering, Huazhong University of Science and Technology, Wuhan, 430074, China
[b] Changjiang Institute of Survey, Planning, Design and Research, Wuhan, 430010, China

ARTICLE INFO

Keywords:
Photovoltaic (PV)
Proton exchange membrane electrolyzer (PEM electrolyzer)
Power allocation
Sequence control strategy

ABSTRACT

For renewable energy driven off-grid hydrogen generation systems, the intermittent and instability nature significantly hinders the electrolyzers' service life and operation safety. Here a variable-periodsequence control strategy is developed for an off-grid photovoltaic-PEM electrolyzer hydrogen generation system via multi-layer DC-DC converters, which control power allocation for the PEM electrolyzer according to the accumulated operation durations under different operation states. The dynamic performance under the fixed and variable period sequence control strategies are systematically investigated. Under the fixed period sequence control strategy, less electrolyzer number contributes to deducing standard deviations of rated/fluctuating power operation durations. Under the variable period sequence control strategies, the standard deviations of the operation duration under the rated and fluctuating power state both are much smaller than those under the fixed period sequence control strategy. When longer sequence period employed at higher solar radiation intensity, the minimum standard deviations of the operation duration under the rated and fluctuating power states are decreased by 28.0% and 44.8%, respectively. When longer sequence period employed at lower solar radiation intensity, the minimum standard deviations are decreased by 49.7% and 51.3%, respectively. The variable sequence control strategy can better allocate electrolyzers' operation states and improve the system operation conditions.

1. Introduction

Global environmental concerns and growing energy demand have sparked the exploitation for clean and green energy substitution [1]. Hydrogen energy plays an important role in achieving sustainable development for its high energy release and pollution-free byproducts. Other than catalytic recombination of hydrocarbons [2], electrolysis of water for hydrogen generation is promising, especially when the electricity produced from renewable energy employed. Among various types of electrolyzers, proton exchange membrane (PEM) electrolyzer presents advantages of high purity of hydrogen production, safety, and operation stability, which could withstand high positive and cathode pressure difference.

Photovoltaic (PV) power generation offers an efficient way to utilize solar energy. Hybrid systems composed of photovoltaic generators, electrolyzers, and auxiliary equipment have been proposed and analyzed [3–8]. Arriaga et al. [9] constructed a hybrid system consisting of a solar panel and a solid polymer electrolyte electrolyzer. The first solar energy to hydrogen hybrid system in China was installed in Tsinghua University [10]. Frano Barbir et al. [11] investigated many possible applications of using PEM electrolyzers to produce hydrogen from renewable energy. Nelson Kelly et al. [12,13] explored the possibility of the realization of hydrogen generation from solar energy for fuel cell electric vehicles. Much efforts have been devoted to the optimization of solar-powered hydrogen generation systems [14,15]. The maximum photovoltaic power coupling can be achieved by finding the best series and parallel combination of photovoltaic panel and electrolyzers. Mathematical methods based on experimental data have also been developed to improve performance of solar-powered hydrogen generation systems [16,17]. In addition, attentions have also been drawn to the economics of generating hydrogen from renewable energy [18–20].

Recently, much efforts have been focused on the improvement of the performance of renewable energy powered hydrogen production systems via the aspect of control strategies. Advanced energy management

* Corresponding author.
** Corresponding author.
E-mail addresses: r_long@hust.edu.cn (R. Long), zcliu@hust.edu.cn (Z. Liu).

https://doi.org/10.1016/j.renene.2023.119074
Received 8 February 2023; Received in revised form 20 June 2023; Accepted 21 July 2023
Available online 23 July 2023

Nomenclature

A	Active area of MEA, cm^2
C	Concentration, mol m^{-3}
D	Diffusion coefficient, m^2 s^{-1}
E	Cell reversible potential, V
F	Faraday constant, C mol $^{-1}$
G	Surface irradiance, W m^2
K_I	Short circuit current coefficient Subscripts and superscripts
K_V	Open circuit current coefficient
M	Molar mass, g mol^{-1}
P	Pressure, bar
R	Resistance, ohm Universal gas constant, J mol^{-1} K^{-1}
T	Temperature, K
V	Voltage, V
I	Current, A
a	Diode ideality factor
a_{H_2O}	Water activity
i	Current density, A cm^{-2}
i_0	Exchange current density, A cm^{-2}
k	Boltzmann constant, J K^{-1}
n	Molar flux, mol m^{-2} s^{-1}
p	Partial pressure, bar
q	Electron charge, C
r	Average pore radius
α	Charge transfer coefficient
δ	Thickness, mm
Ω	Diffusion collision integral
ε	Porosity
ξ	Tortuosity
λ	Degree of humidification
s	Series
p	Parallel
act	Activate
ohm	Ohmic
con	Concentration
an	Anode
cat	Cathode
el	electrode
pl	plate
mem	membrane
eff	efficient

Acronyms

STC	Standard test conditions
SC	Short circuit
OC	Open circuit
PV	photovoltaic

and control strategies have been proved to be feasible to improve the equivalent service life and power regulation characteristics of electrolyzer system [21–25]. Fang et al. [26] developed a modular adaptive control strategy to smooth the fluctuation of wind power. Valenciaga et al. [27] proposed control strategies fitting the wind condition and the battery's charge state for a hybrid system combining a permanent magnet generator with a lead-acid battery pack as well as an alkaline electrolyzer. Abdelkafi et al. [28] designed an energy management algorithm for a hybrid system coupled with a wind driven generator, fuel cell, electrolyzer, and supercapacitor. Zhou et al. [29] presented a control oriented model, where the control strategy could dominate the power flow and hydrogen flow to guarantee high efficiency. Torreglosa et al. [30] proposed a model predictive control energy regulating strategy for the off-grid hybrid system. Won et al. [31] investigated the optimal allocation and operation of a hydrogen generation system powered by renewable energy. Haruni et al. [32] proposed an energy management and power regulation system, which was highly effective at preventing blackouts under low wind conditions or with insufficient energy reserves. Gu et al. [33] developed a smart decentralized control strategy for distributed power generation and energy storage batteries. Gabrielgarciaclua et al. [34] investigated a hybrid hydrogen production system with solar panel array connected to an alkaline electrolyzer directly through a single DC-DC converter and proposed a controller based on hybrid control theory to maximize hydrogen production. Trifkovic et al. [35] investigated a hybrid hydrogen production system with different coupled renewable energy, where electricity was generated by photovoltaic arrays and wind turbine and a two-level control system was adopted to balance the power between discontinuous renewable generation and hydrogen production. Detailed comparisons of control strategies for hybrid solar and wind driven hydrogen generation systems could be found in Table 1.

As listed in Table 1, although much studies have been dedicated to the control strategy for solar or wind energy driven off-grid hydrogen generation systems. Many control strategies have been proposed and analyzed. Efficient control strategy for running the electrolyzer arrays with practically simple operation are highly demanded. In this study, an off-grid photovoltaic electrolysis hydrogen generation system was analyzed, which couples the PV arrays with PEM electrolyzers via multi-layer DC-DC converters. The off-grid hydrogen generation system works under three kinds of operation states according to the real-time solar radiation intensity: high power operation state with no overload, low power operation state with no overload, and overload operation state. Here a variable-period sequence control strategy is developed for an off-grid photovoltaic-PEM electrolyzer hydrogen generation system via multi-layer DC-DC converters, which control power allocation for the PEM electrolyzer according to the accumulated operation durations under different operation states. In the sequence control strategy, each PEM electrolyzer is numbered and is arranged to work in a certain situation (shut-down, fluctuating load, rated load, and overload). Over a given sequence period, the working situation of each PEM electrolyzer rotates sequentially according to their accumulated operation durations of different working conditions, thus to average the total working period

Table 1
Control strategies for some hydrogen production systems.

References	Hydrogen production system	Control strategy
[21]	Wind-PEM system	predictive and reactive power management strategies (PMS)
[22]	PV/wind-PEM system	PMS based on State of Charge of the accumulator (SOC)
[23]	PV-PEM system	Optimal energy management strategy
[26]	Wind-alkaline electrolyzer system	Modular adaptive control strategy
[27]	Wind-alkaline electrolyzer system	Two-level hierarchy control scheme
[28]	Hybrid power production system	Power supervision strategy
[30]	PV/wind turbine/hydrogen/battery hybrid system	Model predictive control (MPC)
[32]	Renewable hybrid power system	Control strategy based on two-level structure
[33]	DC microgrid with multiple renewable distributed generators and energy storage systems.	Mode-adaptive decentralized control strategy
[34]	PV-alkaline electrolyzer system	Hybrid control
[35]	Renewable energy hybrid system	Two-level control system

of each PEM electrolyzer under different working conditions and prolong the service life. The performance under the fixed and variable period sequence control strategies are systematically investigated and analyzed via the MATLAB/Simulink software. Finally, some useful conclusions are drawn.

2. Model description

Fig. 1 illustrates the schematic configuration of an off-grid PV-PEM electrolyzer hydrogen generation system, which contains a PV module, DC-DC converters, and PEM electrolyzer array. DC-DC buck converters are used to connect the PV module to the DC bus under the maximum power point tracking (MPPT) control. Each PEM electrolyzer is connected to the DC bus separately using DC-DC converters. The DC-DC converters between PEM electrolyzers and DC bus are employed to allocate the power for the PEM electrolyzers under the sequence control strategy.

2.1. PV model

Here, a single-diode model is adopted to describe the characteristics of the PV module, as shown in Fig. 2. The output current is given by [36].

$$I = I_{PV} - I_0\left[exp\left(\frac{V+IR_S}{aV_T}\right)-1\right]-\frac{V+IR_s}{R_P} \tag{1}$$

where I_{PV} stands for the light current generated by solar radiation; I_0 is the reverse saturation current of the diode; V is the output voltage; R_s represents the effective series resistance and R_p represents the effective parallel resistance; $V_T = N_s kT/q$ is the thermal voltage of the PV module; N_s is the number of cells connected in series; $k = 1.3806503\times 10^{-23} J/K$ is the Boltzmann constant; $q = 1.60217646 \times 10^{-19}$C is the electron charge; a denotes the diode ideality factor; T denotes the temperature of the p-n junction. I_{PV} can be calculated by [36,37]

$$I_{PV} = I_{PV\_STC} + K_I(T - T_{STC})\frac{G}{G_{STC}} \tag{2}$$

where I_{PV_STC} represents the light current generated by solar irradiation at standard test conditions (STC). G is the irradiance at the surface of the module and $G_{STC} = 1000\ W/m^2$; T is the ambient temperature and $T_{STC} = 298.15$K;, K_I is a temperature coefficient in short current state.

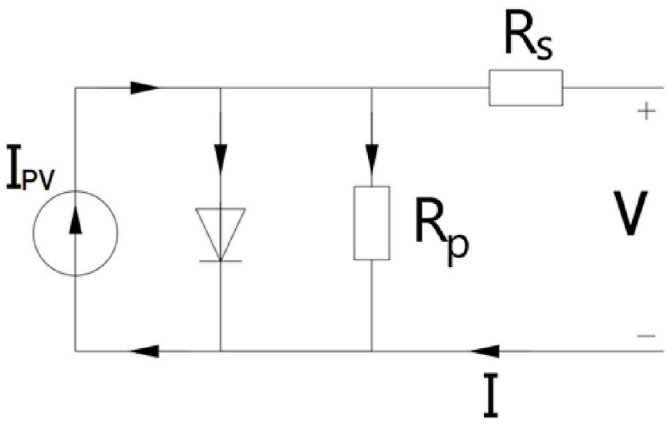

Fig. 2. Circuit diagram of a single-diode PV model.

Considering the temperature variation, the saturation current is given by [38].

$$I_0 = \frac{I_{SC\_STC} + K_I(T - T_{STC})}{exp\left(\frac{V_{OC\_STC}+K_V(T-T_{STC})}{aV_T}\right)-1} \tag{3}$$

where K_V denotes the temperature coefficient in open circuit state.

2.2. PEM electrolyzer model

Different reactions take place between two porous electrodes of PEM electrolyzers:

Anode: $H_2O \rightarrow 2H^+ + \frac{1}{2}O_2 + 2e^-$.

Cathode: $2H^+ + 2e^- \rightarrow H_2$.

The molar flow rate of hydrogen at the cathode side can be calculated as

$$n_{H_2} = \frac{iA}{2F} \tag{4}$$

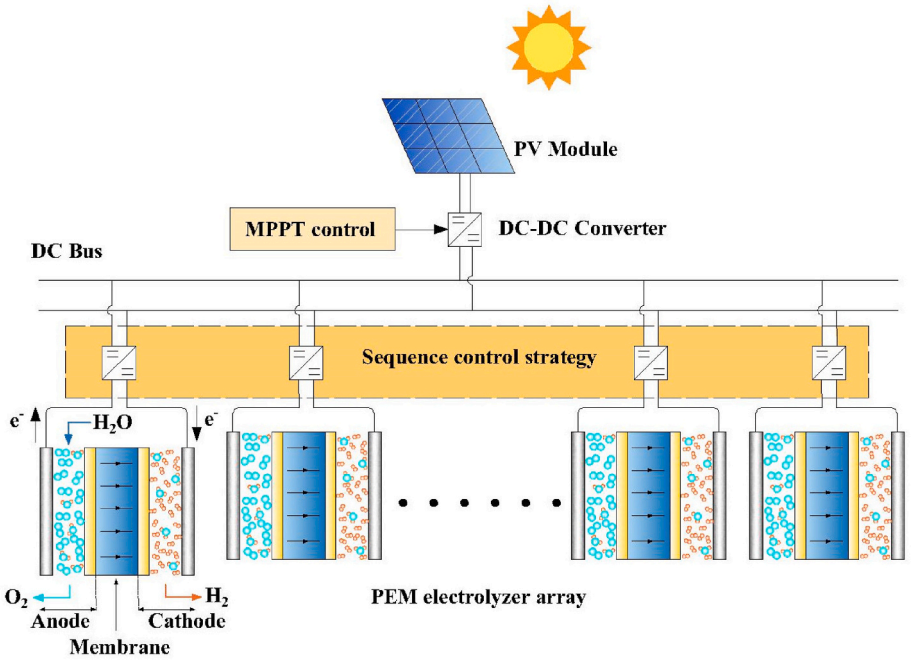

Fig. 1. Off-grid PV-PEM electrolyzer hydrogen generation system.

where i represents the electrolyzer current density; F stands for the Faraday constant; A is the surface area.

The total operating voltage of a PEM electrolyzer is calculated by

$$V = V_{oc} + V_{act} + V_{ohm} + V_{con} \tag{5}$$

where V_{oc}, V_{act}, V_{ohm}, and V_{con} is the open circuit voltage, activation overpotential, ohmic overpotential and concentration overpotential, respectively. According to Nernst equation, the open circuit voltage can be described as [39,40]

$$V_{oc} = 1.229 - 0.9 \times 10^{-3}(T - 298) + \frac{RT}{2F}\left[ln\left(\frac{p_{H_2}\sqrt{p_{o_2}}}{a_{H_2O}}\right)\right] \tag{6}$$

where R stands for the gas constant; T is the electrolyzer temperature under working condition; p_{H_2} and p_{o_2} are the partial pressures of hydrogen and oxygen, respectively; a_{H_2O} represents the water activity.

Activation overpotential represents the losses in the electrochemical process. Protons and electrons must overcome additional potential to transfer through membrane and electrodes.

$$V_{act} = V_{act,an} + V_{act,cat} \tag{7}$$

$$V_{act,j} = \frac{RT}{\alpha_j F}\sin h^{-1}\left(\frac{i}{2i_{0,j}}\right) \quad j = an, cat \tag{8}$$

where α_j stands for charge transfer coefficient of the anode and cathode; $i_{0,j}$ represents the exchange current density of the anode and cathode [41].

The ohmic overpotential originates from the electrode surfaces, membrane and bipolar plates resistances [42].

$$V_{ohm} = \left(R_{el} + R_{pl} + R_{mem}\right)iA \tag{9}$$

where R_{el} is the electrode resistance, R_{pl} is the bipolar resistance and R_{mem} is the membrane resistance.

$$R_{el,pl} = \rho_{eff}\frac{l}{A} \tag{10}$$

$$R_{mem} = \frac{\delta_{mem}}{A\sigma_{mem}} \tag{11}$$

where ρ_{eff} is the effective electrical resistivity of the electrodes; l is the electrons path length; δ_{mem} is the membrane thickness and σ_{mem} is the membrane conductivity given by [43]

$$\sigma_{mem} = (0.005139\lambda - 0.00326)\left[1268\left(\frac{1}{303} - \frac{1}{T}\right)\right] \tag{12}$$

where λ represents the water content of the membrane.

During electrolysis process, the alteration in concentration of the reactants at the electrode surface causes the concentration overpotential. The concentration overpotential can be expressed as

$$V_{con} = \frac{RT}{4F}ln\frac{C^{mem}_{O_2}}{C^{mem}_{O_2,0}} + \frac{RT}{2F}ln\frac{C^{mem}_{H_2}}{C^{mem}_{H_2,0}} \tag{13}$$

where $C^{mem}_{O_2}$ and $C^{mem}_{H_2}$ are the concentration of oxygen and hydrogen at the membrane-electrode junction, respectively [44].

$$C^{mem}_{H_2} = \frac{P_{cat}X_{H_2}}{RT} + \frac{\delta^{cat}_{el}n_{H_2}}{D^{cat}_{eff}} \tag{14}$$

$$C^{mem}_{O_2} = \frac{P_{an}X_{O_2}}{RT} + \frac{\delta^{an}_{el}n_{O_2}}{D^{an}_{eff}} \tag{15}$$

where X_{H_2} and X_{O_2} are the amount of molar fraction of hydrogen and oxygen; P_{cat} and P_{an} are the pressure at the cathode and anode, respectively; δ_{el} is the electrode thickness. D^{cat}_{eff} and D^{an}_{eff} are the effective diffusion coefficient of the cathode and anode, respectively, which can be calculated as [45]

$$\frac{1}{D^{cat}_{eff}} = \frac{\varepsilon}{\xi}\left(\frac{1}{D^{H_2-H_2O}_{eff}} + \frac{1}{D^{H_2O,K}_{eff}}\right) \tag{16}$$

$$\frac{1}{D^{an}_{eff}} = \frac{\varepsilon}{\xi}\left(\frac{1}{D^{O_2-H_2O}_{eff}} + \frac{1}{D^{H_2O,K}_{eff}}\right) \tag{17}$$

where ε/ξ is the ratio of electrode porosity to tortuosity; $D^{H_2-H_2O}_{eff}$ and $D^{O_2-H_2O}_{eff}$ are the effective molecular diffusion coefficient for binary system of $H_2 - H_2O$ and $O_2 - H_2O$; $D^{H_2O,K}_{eff}$ is the effective Knudsen diffusion coefficient for water [46,47].

$$D^{H_2-H_2O}_{eff} = 0.0013\left(\frac{1}{M_{H_2}} + \frac{1}{M_{H_2O}}\right)^{1/2}\frac{T^{3/2}}{P_{cat}\sigma^2_{H_2-H_2O}\Omega_D} \tag{18}$$

$$D^{O_2-H_2O}_{eff} = 0.0013\left(\frac{1}{M_{O_2}} + \frac{1}{M_{H_2O}}\right)^{1/2}\frac{T^{3/2}}{P_{an}\sigma^2_{O_2-H_2O}\Omega_D} \tag{19}$$

$$D^{H_2O,K}_{eff} = \frac{4}{3}r\sqrt{\frac{8RT}{\pi M_{H_2O}}} \tag{20}$$

where M_{H_2} and M_{O_2} are the molar weights of H_2 and O_2; r is the average pore radius; $\sigma_{H_2-H_2O}$ and $\sigma_{O_2-H_2O}$ are the mean radius of binary molecules of $H_2 - H_2O$ and $O_2 - H_2O$; Ω_D is the dimensionless diffusion collision integral [48]

$$\Omega_D = \frac{1.06}{\tau^{0.156}} + \frac{0.193}{exp(0.47\tau)} + \frac{1.036}{exp(1.53\tau)} + \frac{1.765}{3.894\tau} \tag{21}$$

$$\sigma_{H_2-H_2O} = \frac{\sigma_{H_2} + \sigma_{H_2O}}{2} \tag{22}$$

$$\sigma_{O_2-H_2O} = \frac{\sigma_{O_2} + \sigma_{H_2O}}{2} \tag{23}$$

$$\tau_{H_2-H_2O} = \frac{kT}{\varepsilon_{H_2-H_2O}} \tag{24}$$

$$\tau_{O_2-H_2O} = \frac{kT}{\varepsilon_{O_2-H_2O}} \tag{25}$$

where $\varepsilon_{H_2-H_2O}$ and $\varepsilon_{O_2-H_2O}$ are the Lennard-Jones energies

$$\varepsilon_{H_2-H_2O} = \sqrt{\varepsilon_{H_2}\varepsilon_{H_2O}} \tag{26}$$

$$\varepsilon_{O_2-H_2O} = \sqrt{\varepsilon_{O_2}\varepsilon_{H_2O}} \tag{27}$$

where σ_i for H_2, O_2 and H_2O are 2.827 $\dot{A}$, 3.467 $\dot{A}$ and 2.641 $\dot{A}$, respectively [49]. ε_i/k for H_2, O_2 and H_2O are 59.7K, 106.7K and 809.1K.

2.3. DC-DC buck converter model

As shown in Fig. 3, the circuit theory is applied to simulate the open and closed states of DC-DC buck converter.

When the circuit is closed,

$$\begin{cases} L\dfrac{di_L}{dt} = u_i - u_c \\ C\dfrac{du_c}{dt} = i_L - \dfrac{u_c}{R} \end{cases} \tag{28a}$$

When the circuit is open

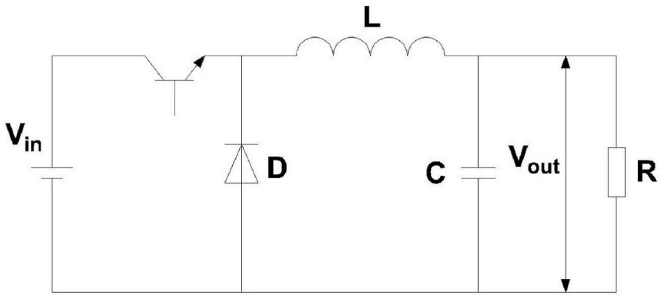

Fig. 3. Schematic diagram of the DC-DC buck converter.

$$\begin{cases} L\dfrac{di_L}{dt} = -u_c \\ C\dfrac{du_c}{dt} = i_L - \dfrac{u_c}{R} \end{cases} \tag{29a}$$

Taking duty cycle d into consideration yields to

$$\begin{cases} L\dfrac{di_L}{dt} = Du_i - u_c \\ i_L = C\dfrac{du_c}{dt} + \dfrac{u_c}{R} \end{cases} \tag{30a}$$

L in the circuit can be designed by the condition [50].

$$L \geq \frac{V_{out}}{k_{\Delta i} \bullet f \bullet I_{out(min)}} \bullet \left(1 - \frac{V_{out}}{V_{in}}\right) = \frac{R_{out(max)} \bullet (1-d)}{k_{\Delta i} \bullet f} \tag{31a}$$

where $k_{\Delta i} = \Delta i_L / I_{out}$ is the ripple coefficient, which is usually 20%–50%; f is the frequency of the pulse-width modulated pulses; $d = V_{out}/V_{in}$ is the duty cycle. As for the buck converter between PV module and DC Bus-bar, $V_{out} = V_{Bus}$ is the DC Bus voltage. R_{out} is determined by MPPT control of the PV module:

$$R_{out(max)} = \frac{V_{out}}{P_{MPP(min)}} \tag{32a}$$

where $P_{MPP(min)}$ is the minimum power provided by the PV module.

The filter capacitor can be chosen by the following expression:

$$C \geq \frac{(1-d)}{8 \bullet L \bullet f^2 \bullet k_{\Delta V_{out}}} \tag{33a}$$

where $k_{\Delta V_{out}} = \Delta V_{out}/V_{out}$ is the ripple coefficient of the output voltage, which is usually 1%–5%.

2.4. Sequence control strategy

The sequence control strategy is employed here to allocate the power generated in the PV module to the PEM electrolyzer arrays. The PEM electrolyzers are numbered, and a certain sequence period T is set. One electrolyzer is arranged to work under the fluctuation power. The rest of electrolyzers is arranged to work at the rated power or be shut-down state according to the real-time value of the solar radiation intensity. Every after the sequence period T, the electrolyzers works either under the rated power state, fluctuation power state or the shutdown state alternately. Correspondingly, the power for each numbered electrolyzer is allocated. The schematic diagram of sequence strategy is depicted in Fig. 4. Compared with the simple "equalizing" control strategy, the input power can be allocated in a small number of cells, thus to avoid the electrolyzers working far from the safe operating condition as well as reducing the risk of operation accidents.

The sequence control strategy aims to provide an alternative scheme for improving service life of the electrolyzers in the photovoltaic-PEM electrolyzer hydrogen generation system. The operation duration of each electrolyzer under different operating conditions is balanced. The

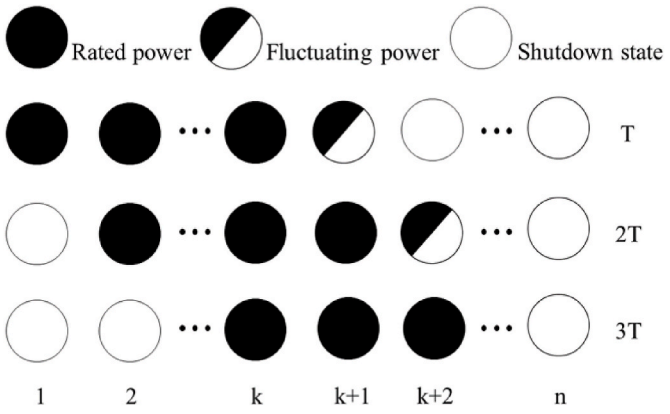

Fig. 4. Schematic diagram of the sequence control strategy.

number of electrolyzers working in this sequence strategy is n; the rated power of each electrolyzer is P_e, the fluctuating power is P_b; and the actual power is $P_{el,i}$, where i is the serial number of the electrolyzer. The total rated power of the electrolyzer array is P_{el}, and the photovoltaic power is P_{sun}. The flow diagram of the sequence control strategy of the PV-PEM electrolyzer array system is illustrated in Fig. 5. The working conditions of the electrolyzers can be divided into the following three situations:

Situation 1: High power operation state with no overload.

In this situation, $P_{sun} < P_{el}$, only one electrolyzer works in the fluctuating power state; And the other (n-1) electrolyzers work in the rated power state, thus the whole array of electrolyzers works in the high power operation state without overload. The working time of the i-th electrolyzer is T_i. At first

$$\begin{cases} P_{sun} = (n-1)P_e + P_b \\ P_{el,1} = P_{el,2} == P_{el,n-1} = P_e \\ P_{el,n} = P_b \end{cases} \tag{28b}$$

When the working time of the electrolyzer under fluctuating power state reaches the sequence period, that is, $T_i = T$. The power of each electrolyzer is rotated in turn according to its number

$$\begin{cases} P_{el,2} = P_{el,3} == P_{el,n} = P_e \\ P_{el,1} = P_b \end{cases} \tag{29b}$$

Situation 2: Low power operation state with no overload.

In this situation, one electrolyzer works in the state of fluctuating power; The number of electrolyzers working at rated power state is less than n-1; the remaining m electrolyzers are in the shutdown state, and the electrolyzer array works in the condition of no overload and low

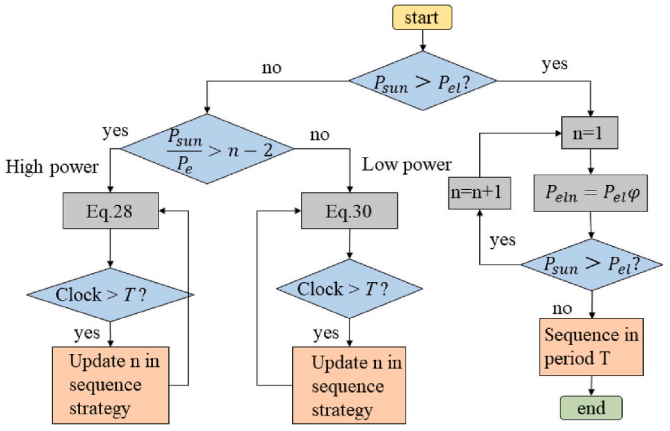

Fig. 5. Flow diagram of the sequence control strategy.

power. At first

$$\begin{cases} P_{sun} = (n-m-1)P_e + P_b \\ P_{el,1} = P_{el,2} == P_{el,n-m-1} = P_e \\ P_{el,n-m} = P_b \\ P_{el,n-m+1} = \cdots = P_{el,n} = 0 \end{cases} \tag{30b}$$

When the working time of the electrolyzer under the fluctuating power state reaches the sequence period, the accolated power of each electrolyzer is rotated in turn according to its number.

$$\begin{cases} P_{el,2} = P_{el,3} = \cdots = P_{el,n-m} = P_e \\ P_{el,n-m+1} = P_b \\ P_{el,n-m+2} = \cdots = P_{el,n} = P_{el,1} = 0 \end{cases} \tag{31b}$$

Situation 3: Overload operation state.

Under this operating condition, $P_{sun} > P_{el}$. Since the solar photovoltaic power is higher than the total rated power of all electrolyzers, it is necessary to select some electrolyzers to work at the overload power state. Firstly, the power $P_{el,1}$ of the No. 1 electrolyzer in the cyclic queue is increased to φ (overload coefficient) times of the rated power P_e, thus it is in the overload operate state. The No. 2 electrolyzer is also changed to the overload operation state, and the rest can be done in the same manner until all the electrolyzers are in the overload operate state. Assuming that the number of electrolyzers operating in overload state is k, and the other electrolyzers are in rated power operation state, then

$$\begin{cases} P_{sun} = k\varphi P_e + (n-k-1)P_e + P_b \\ P_{el1} = P_{el2} = \cdots = P_{elk} = \varphi P_e \\ P_{elk+1} = P_b \\ P_{elk+2} = \cdots = P_{eln} = P_e \end{cases} \tag{32b}$$

After the number of electrolyzers working in overload state is determined, according to the sequence control strategy, when the operation duration of electrolyzers reaches the sequence period, that is, $T_n = T$, the power of each electrolyzer is rotated in turn according to its number to realize the sequence in overload state.

$$\begin{cases} P_{el,2} = P_{el,3} = \cdots = P_{el,k+1} = \varphi P_e \\ P_{el,k+2} = P_b \\ P_{el,k+3} = \cdots = P_{el,n} = P_{el,1} = P_e \end{cases} \tag{33b}$$

3. Results and discussion

3.1. Model validation

The PV model here is validated using the experiment data of a chosen PV system (MSX-60) [51]. Table 2 lists the parameters of the PV modules [38]. The comparison was made at a temperature of 25 °C. The operating current calculated via the PV model in this paper and the experimental data under different operating voltages are compared. As shown in Fig. 6, the maximum error deviation between the model and experiment data is 1.04%. The model adopted here shows great accordance with the experimental data. The parameters of the PEM electrolyzer model employed here are summarized in Table 3. The operating voltage calculated via the PEM model described here and the simulating data of Abdin under different current density are compared [52]. Fig. 6 shows the comparison of the calculated polarization curve at 55 °C, 10 bar (cathode) and the simulating results of Ref. [52]. The maximum error deviation between the model and simulating results of Ref. is 1.94%, which validates the PEM electrolyzer model in present study.

Table 2
Parameters of the PV model and the DC-DC buck converter model.

Parameter	Value
I_{PV_STC}	3.803 A
I_{SC_STC}	3.8 A
V_{OC_STC}	21.1 V
K_I	3 mA/ °C
K_V	−80 mV/ °C
N_s	36
a	1.3
R_s	304.83 Ω
R_P	0.2 Ω
C	100 μ F
L	200 μF
f	10 kHz
V_{Bus}	6 V

3.2. Performance under fixed period sequence control strategy

Here, the output voltage of PV module is set at 17.5V and the operation temperature is 25 °C. The rated current density of PEM electrolyzer is 1.2 A/ cm^2 and the operation temperature is 55 °C. The number of PV cells and PEM electrolyzers working in the system are 30 and 6. The intensity of light radiation is governed by Equation (34). The solar radiation intensity before 6:30 and after 17:30 is too low. Therefore, the PEM electrolyzers are in the shut-down state.

$$G = \begin{cases} 0, 0 < t < 6 \\ -3 + 0.66667t - 0.02778t^2, 6 \le t \le 18 \\ 0, 18 < t < 24 \end{cases} \tag{34}$$

At the fixed period time $T = 300$s, the daily allocated power of the six electrolyzers is shown in Fig. 7. The daily hydrogen production rate of the six electrolyzers is shown in Fig. 8. All the six electrolyzers did not reach the overload power state. The maximum power of electrolyzer operation is rated power. The operation durations of the six electrolyzers in rated power state are 4.0208 h, 3.9675 h, 3.9167 h, 3.9167 h, 3.8939 h and 3.9486 h, respectively. The average operation duration under the rated power state is 3.9440 h. The standard deviation of the rated power operating time of all electrolyzers is 0.0418h. The operation duration of the six electrolyzers under fluctuating power state are 1.7611 h, 1.8867 h, 1.8842 h, 1.8333 h, 1.8561 h, 1.7786 h, respectively. The average operation duration under the fluctuating power state is 1.8333h. The standard deviation of the fluctuating power operating time of all electrolyzers is 0.0486h. The operation durations under rated power and fluctuating power state of the six electrolyzers are relatively averaged. As shown in Fig. 8, the hydrogen production rate of the six electrolyzers show a similar trend with the power allocated.

As shown in Fig. 9, the total operation duration of different electrolyzers under the rated power state presents no obvious difference. And so does the total operation duration of different electrolyzers under the fluctuating power state. When the number of electrolyzers is 4, the standard deviation of the operation duration under the rated power state is 0.0264 h. When the number of electrolyzers is 8, the standard deviation of operation duration under the fluctuating power state is 0.0298 h. Fig. 9 also shows the influences of the electrolyzer number on switching times of system running state and hydrogen production. More electrolyzers lowered the average switching times of each electrolyzer. When 4 electrolyzers involved, the total switching times is the least, 318 times. The total hydrogen production also exhibits the smallest value, originating from the fact that some electrolyzers working under overload state, which induces significant power loss. When larger number of electrolyzers employed, the operation durations under the overload state are obviously deduced. Therefore, the total hydrogen production presents no obvious difference under various large electrolyzer numbers.

3.3. Performance under variable period sequence control strategy

Since the daily solar radiation intensity varies with time, setting different sequence periods at different solar radiation intensity should be emphasized. Here longer sequence period at higher solar radiation intensity and longer sequence period at lower solar radiation intensity are considered. respectively.

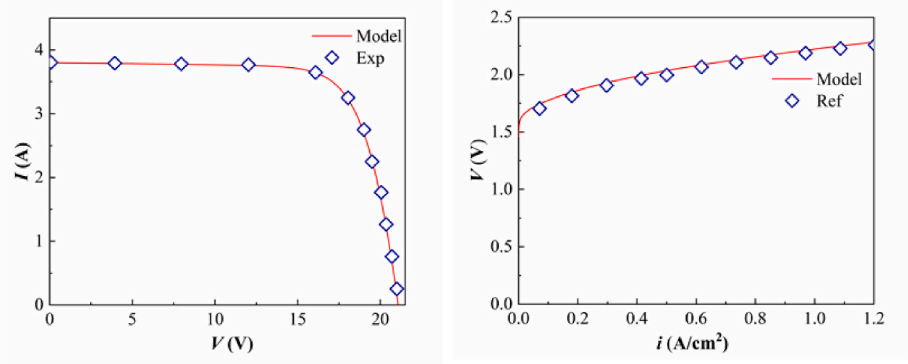

Fig. 6. Validation of the PV and PEM electrolyzer models.

Table 3
Parameters of the PEM electrolyzer model.

Parameter	Value
A	160 cm^2
δ_{mem}	0.0254 cm
δ_{el}	0.008 cm
ε	0.3
ξ	4
F	96,485 C mol^{-1}
R	8.3144 J $mol^{-1}K^{-1}$
r	1 μ m
λ	21
α_{an}	0.8
α_{cat}	0.25
$i_{0,an}$	1×10^{-7} A/cm^2
$i_{0,cat}$	1×10^{-1} A/cm^{-1}
P_{an}	1 bar
P_{cat}	10 bar

3.3.1. *Longer sequence period at higher solar radiation intensity*

Fig. 10 show the daily power variation of six electrolyzers when a longer sequence period at higher solar radiation intensity. Within 6.5h–17.5h, the sequence period T_1 in 0–3.67h and 7.33–11h is set to be 300s. The sequence period T_2 in 3.67–7.33h is set to be 600s. It can be seen that the switch of operation state of the six electrolyzers is less frequent during 3.67–7.33h. The average operation duration of the six electrolyzers under the rated power state is 3.9440h. And the average operation duration under the fluctuating power state is 1.8333h. The standard deviation of operation duration under the rated power state is 0.0623h. The standard deviation of operation duration under the fluctuating power state is 0.0681h. Fig. 11 shows the variation of hydrogen production rate of six electrolyzers. The hydrogen production rate of the six electrolyzers also shows a similar trend with the power allocated.

As shown in Fig. 12, the total operation durations of the involved electrolyzers under the rated and fluctuating power state present no obvious difference at different electrolyzer numbers. At small electrolyzer numbers, their standard deviations increase first with increasing electrolyzer numbers, reaches their maximum values, then decreases. The maximum standard deviation of the operation duration under the rated power state is 0.0736 h when 5 electrolyzers involved. The minimum standard deviation of the operation duration under the rated power state is 0.0198 h when 7 electrolyzers involved. The maximum standard deviation of the operation duration under the fluctuating power state is 0.0744 h when 5 electrolyzers involved, and the minimum one is 0.0595 h when 8 electrolyzers involved. Fig. 12 also shows the influence of the electrolyzer number on the switching times of operating state and hydrogen production. When 4 electrolyzers involved, the total

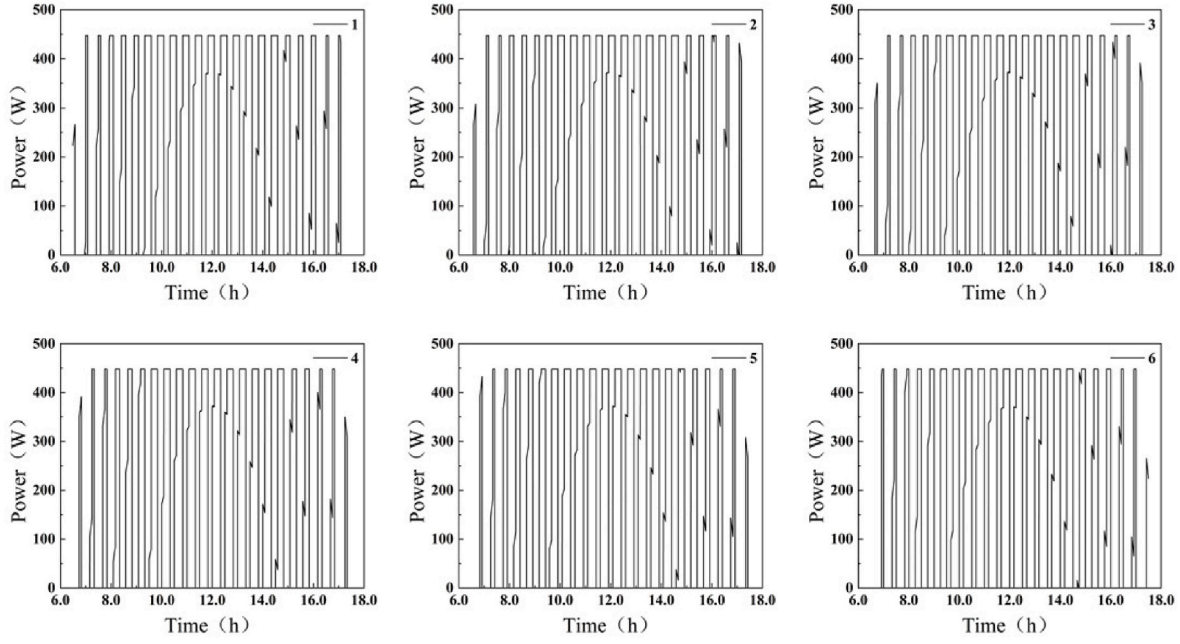

Fig. 7. Daily allocated power of the electrolyzers.

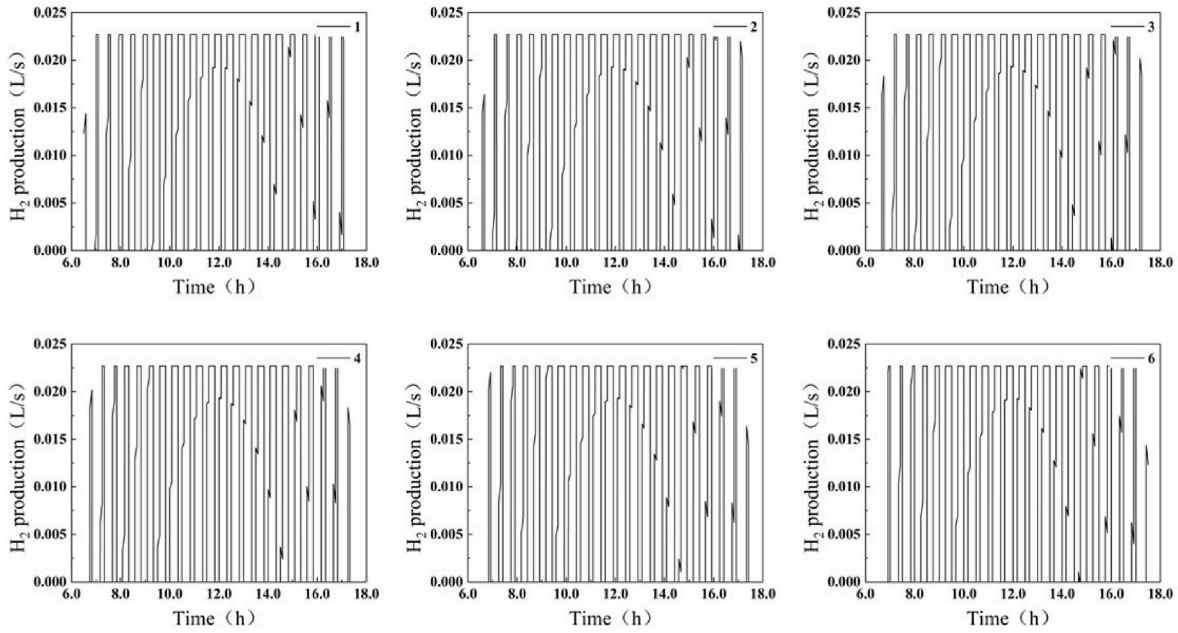

Fig. 8. Daily hydrogen production of the electrolyzers.

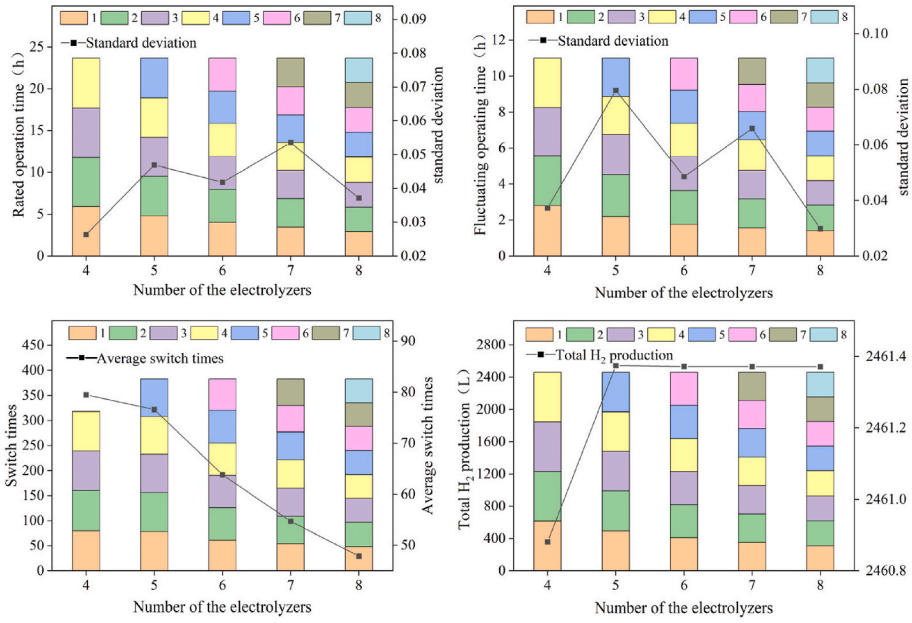

Fig. 9. Influence of electrolyzer number on the elctrolyzer operating duration under the rated power state, fluctuating power state, standard deviation, switching times and hydrogen production.

switch times presents the least value. The total hydrogen production exhibits the smallest value. When larger number of electrolyzers employed, the total hydrogen production presents no obvious difference under various large electrolyzer numbers.

Here the impact of the location of the longer sequence period on the system performance is further analyzed. The longer sequence period is located between the time point T_a and T_b, where a and b are the start point and termination point. As shown in Fig. 13, smaller T_a and larger T_b lead to fewer the average switching times. When $T_a = 5.083$h and $T_b = 8.056$h, the standard deviation of the operation duration under the fluctuating power state is the lowest. The equivalent fixed sequence period is 350s by taking switch times of the operating states into consideration. The system performance under the variable period sequence control strategy and the equivalent fixed period sequence control strategy is compared in Table 4. Under the variable-period sequence control strategy, the standard deviations of the operation duration under the rated power state and the fluctuating power state both are much smaller than those under the fixed-period sequence control strategy. The standard deviations of the operation duration under the rated power state and the fluctuating power state are decreased by 28.0% and 44.8%, respectively.

3.3.2. *Longer sequence period at lower solar radiation intensity*

Fig. 14 show the daily power variation of six electrolyzers when a longer sequence period at lower solar radiation intensity. Within 6.5h–17.5h, the sequence period T_1 in 0–3.67h and 7.33–11h is set to be

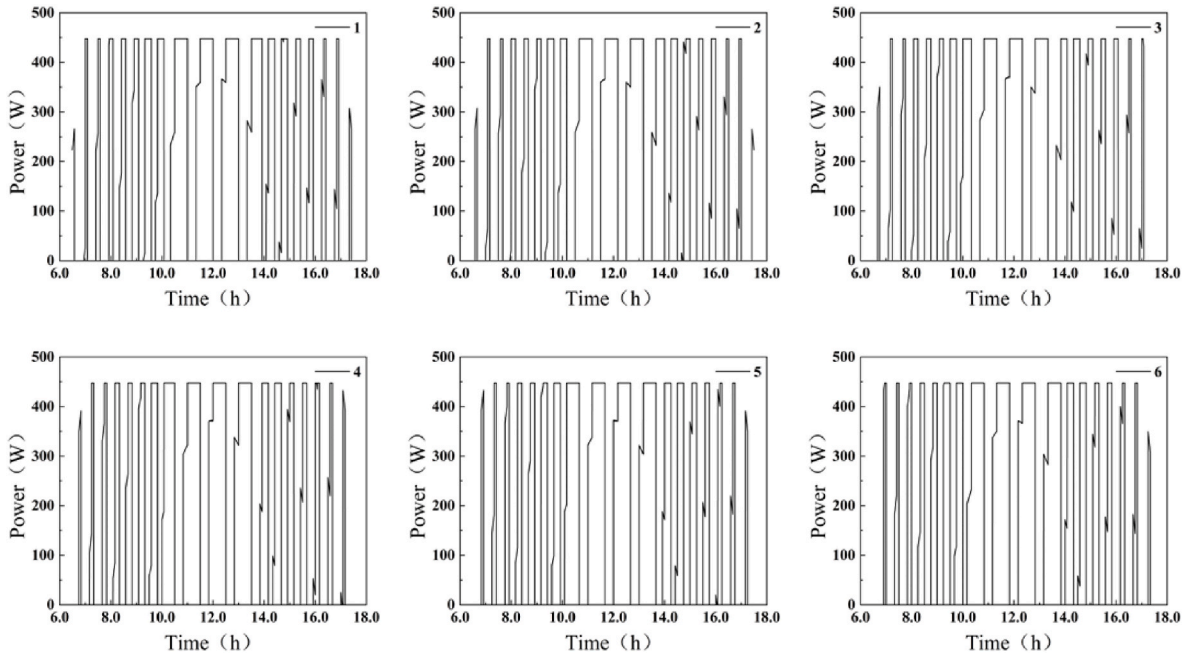

Fig. 10. Daily power allocated for the electrolyzers with longer sequence period at higher solar radiation.

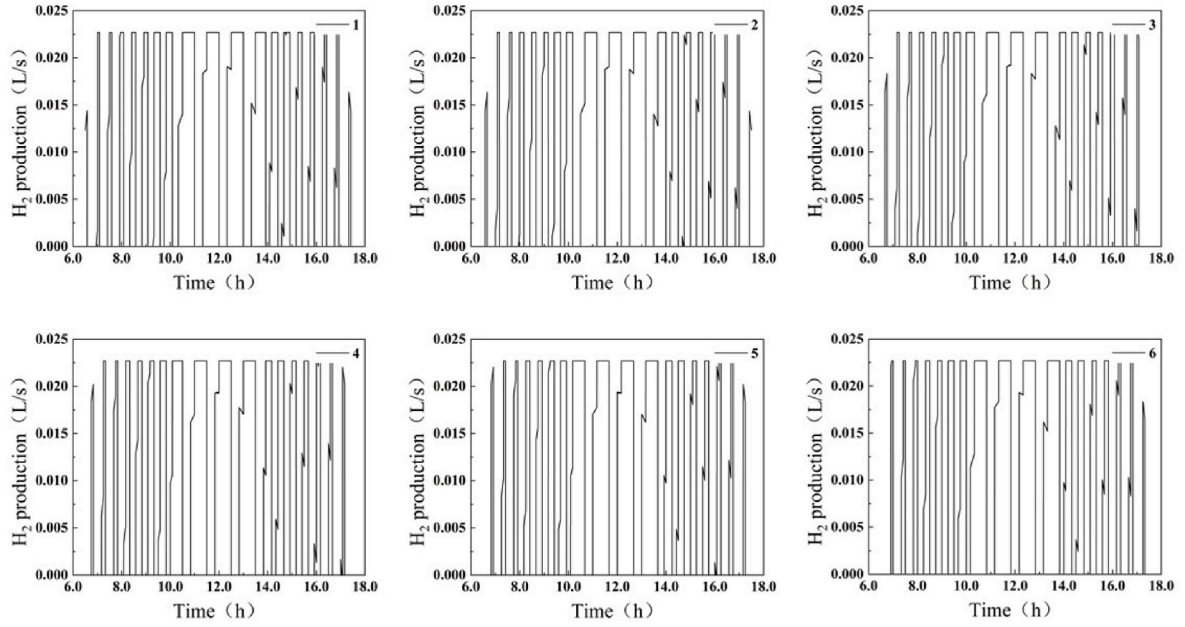

Fig. 11. Hydrogen production rate for the electrolyzers with longer sequence period at higher solar radiation.

600s. The sequence period T_2 in 3.67–7.33h is set to be 300s. It can be seen that the operation state of the six electrolyzers changed more frequently during 3.67–7.33h. The average operation duration of the six electrolyzers under the rated power state is 3.944h. The average operation duration under the fluctuating power state is 1.833h. The standard deviation of operation duration under the rated power state is 0.0481h. The standard deviation of operation duration under the fluctuating power state is 0.1240h. Fig. 15 shows the variation of hydrogen production rate of six electrolyzers. The hydrogen production rate of the six electrolyzers also shows a similar trend with the power allocated.

As shown in Fig. 16, the standard deviations of operation durations under the rated and fluctuating power states decrease first with increasing electrolyzer numbers, reach their minimum values, then increase. The maximum standard deviation of the operation duration under the rated power state is 0.2092 h when 8 electrolyzers involved. The minimum standard deviation of the operation duration under the rated power state is 0.0481 h when 6 electrolyzers involved. The maximum standard deviation of the operation duration under the fluctuating power state is 0.1753 h when 4 electrolyzers involved, and the minimum one is 0.1240 h when 6 electrolyzers involved. Fig. 16 also shows the influence of the electrolyzer number on the switching times of operating state and hydrogen production. The average switching times increases with increasing electrolyzer numbers, reaches its maximum values, then decreases. When 4 electrolyzers involved, the total switch times presents the least value. The total hydrogen production exhibits the smallest value. When larger number of electrolyzers employed, the

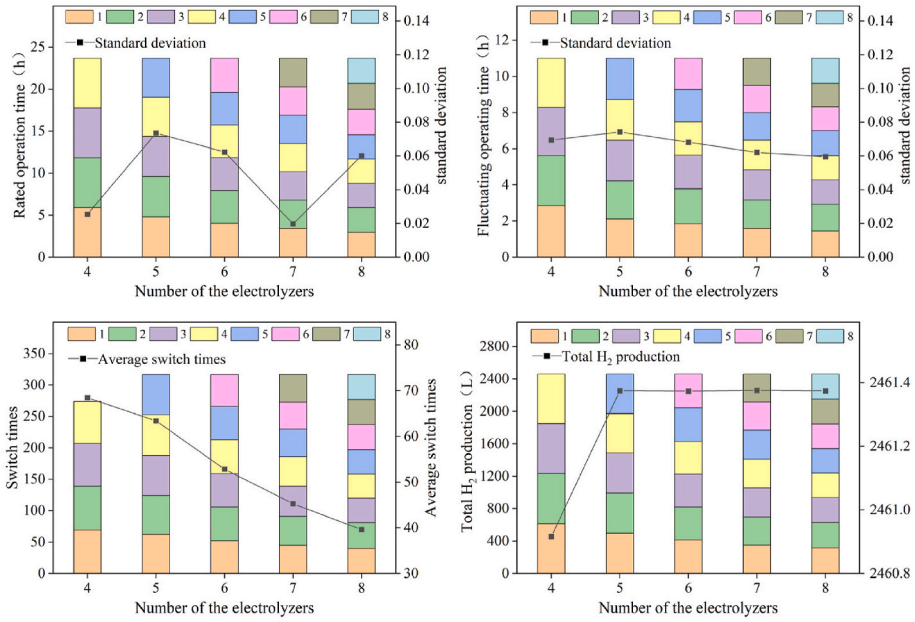

Fig. 12. Influence of electrolyzer number on the elctrolyzer operating duration under the rated power state, fluctuating power state, standard deviation, switching times and hydrogen production with longer sequence period at higher solar radiation.

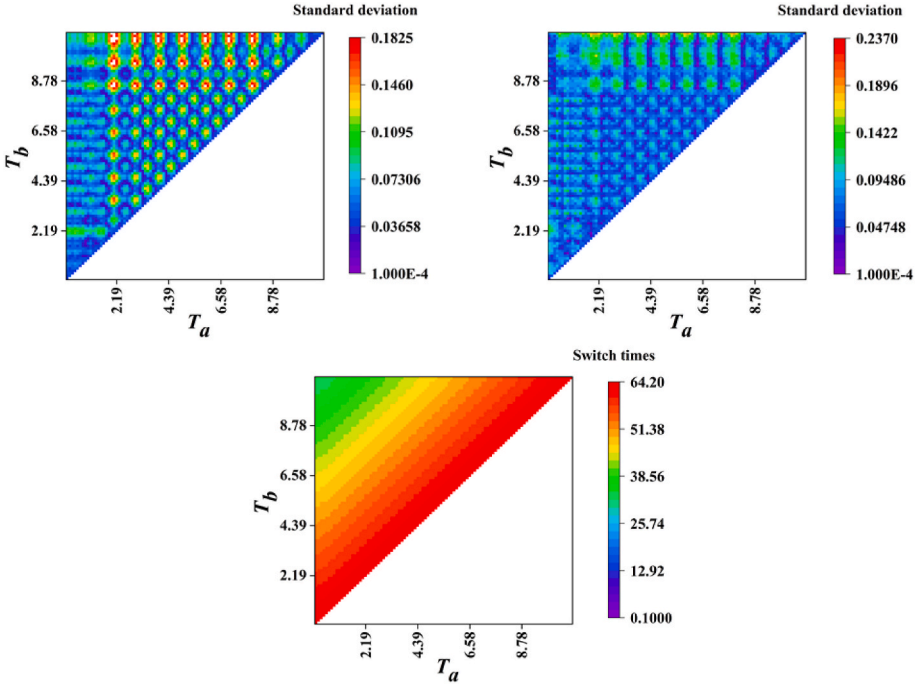

Fig. 13. Hot spot diagrams of standard deviation of operation durations under the rated power state and under the fluctuating power state, and average switching times with longer sequence period at higher solar radiation.

Table 4
Comparison between variable period and fixed period sequence control strategies with longer sequence period at higher solar radiation.

sequence control strategy	Rated power operation duration	Fluctuating power operation duration	Average switch times
Variable period	0.0418	0.0486	54.83
Fixed period	0.0581	0.0881	55

total hydrogen production presents no obvious difference under various large electrolyzer numbers due to relatively small power loss.

Here with longer sequence period at lower solar radiation, the impact of the location of the shorter sequence period on the system performance is also investigated. The shorter sequence period is located between the time point T_a and T_b, where a and b are the start point and termination point. As shown in Fig. 17, larger T_a and smaller T_b lead to fewer average switching times. When $T_a = 2.889$h and $T_b = 8.889$h, the standard deviation of the operation duration under the fluctuating power state is the lowest. The equivalent fixed sequence period is 388s.

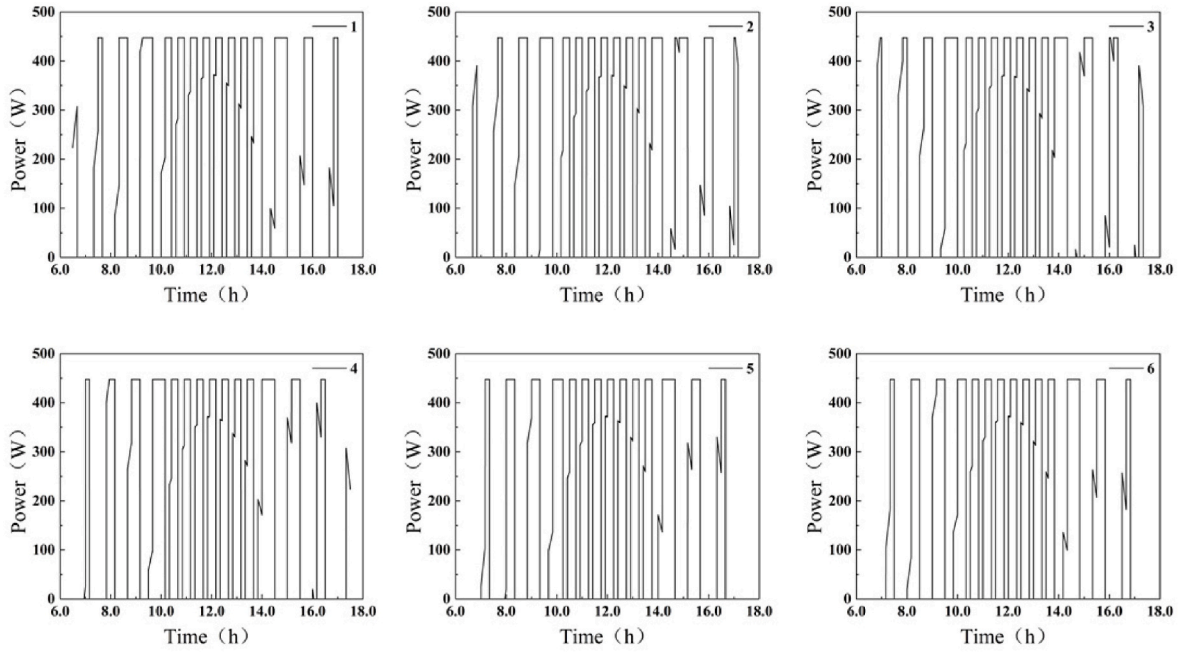

Fig. 14. Daily power allocated for the electrolyzers with longer sequence period at lower solar radiation.

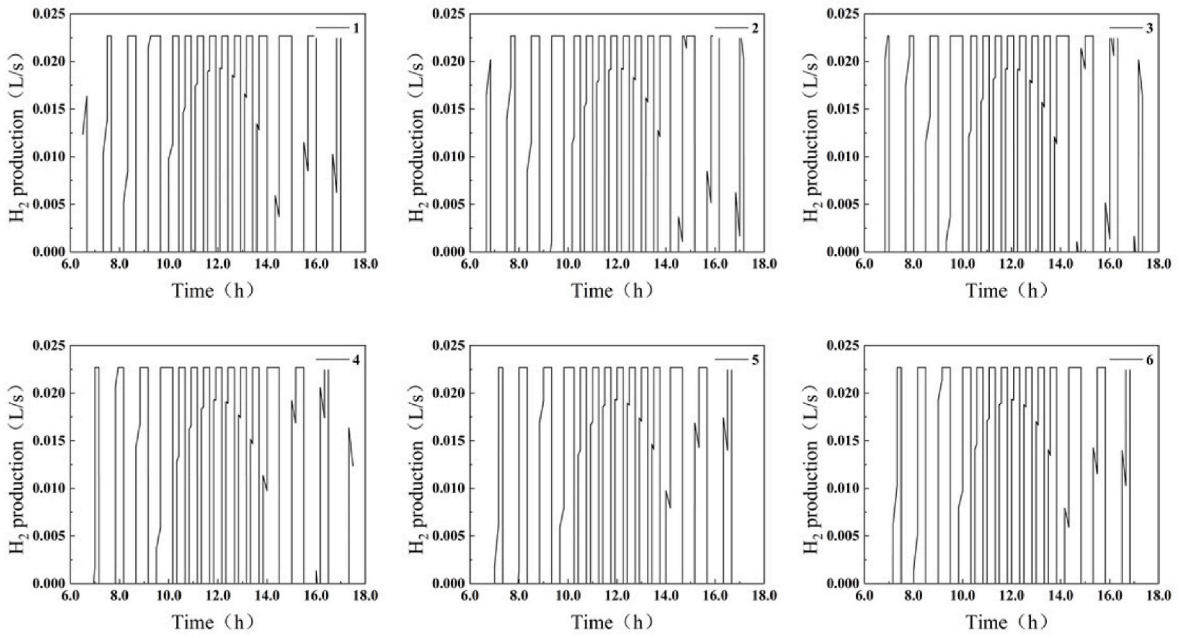

Fig. 15. Hydrogen production rate for the electrolyzers with longer sequence period at lower solar radiation.

The system performance under the variable period sequence control strategy and the equivalent fixed period sequence control strategy is compared in Table 5. Under the variable-period sequence control strategy, the standard deviations of the operation duration under the rated and fluctuating power states both are much smaller than those under the fixed period sequence control strategy. The standard deviations of the operation duration under the rated power state and fluctuating power state are decreased by 49.7% and 51.3%, respectively.

4. Conclusions

In this study, a variable sequence control strategy is developed for an off-grid photovoltaic-PEM electrolyzer hydrogen generation system via multi-layer DC-DC converters, which control power allocation for the PEM electrolyzer according to the accumulated operation durations under different operation states. The dynamic performance under the fixed and variable period sequence control strategies are systematically investigated. The main conclusions are as follows:

(1) With the sequence control strategy applied, the operation durations under the rated and fluctuating power states for different electrolyzers are well averaged. Under the fixed period sequence control strategy, less electrolyzer number contributes to deducing standard deviations of different operation durations.
(2) Under the variable-period sequence control strategies, the total operation duration of the involved electrolyzers under the rated

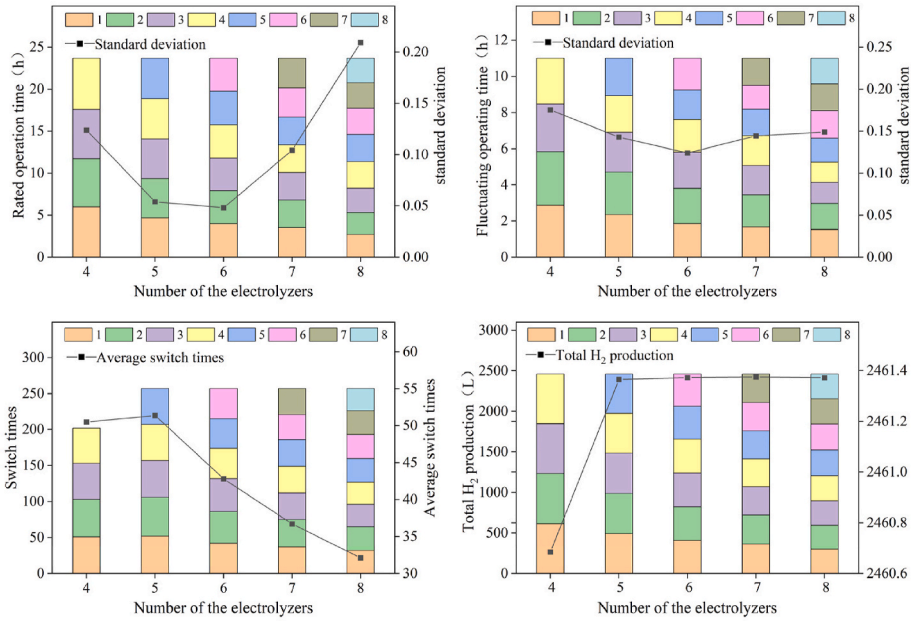

Fig. 16. Influence of electrolyzer number on the elctrolyzer operating duration under the rated power state, fluctuating power state, standard deviation, switching times and hydrogen production with longer sequence period at lower solar radiation.

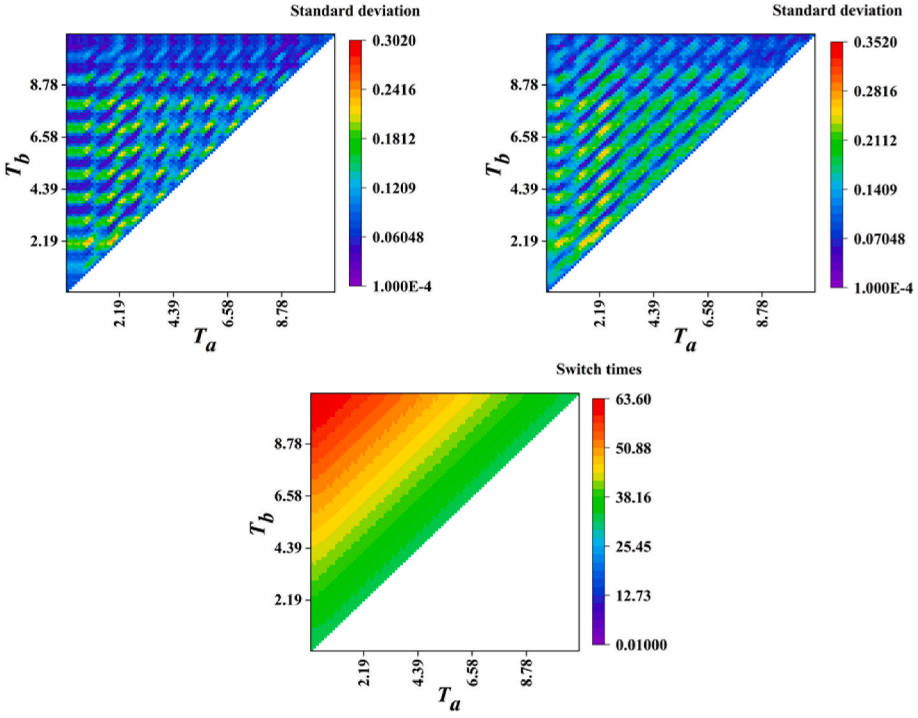

Fig. 17. Hot spot diagrams of standard deviation of operation durations under the rated power state and under the fluctuating power state, and average switching times with longer sequence period at lower solar radiation.

Table 5
Comparison between variable period and fixed period sequence control strategies with longer sequence period at lower solar radiation.

Sequence control strategy	Rated power operation duration	Fluctuating power operation duration	Average switch times
Variable period	0.0460	0.0485	49.83
Fixed period	0.0914	0.0996	49.5

power state and the fluctuating power state present no obvious difference at different electrolyzer numbers. The standard deviations of the operation duration under the rated power state and the fluctuating power state both are much smaller than those under the fixed period sequence control strategy.

(3) When longer sequence period employed at higher solar radiation intensity, compared to the fixed period sequence control strategy, at an electrolyzer number of 6, the minimum standard deviations of the operation duration under the rated and fluctuating power

states are decreased by 28.0% and 44.8%, respectively. When longer sequence period employed at lower solar radiation intensity, at an electrolyzer number of 6, the minimum standard deviations of the operation duration under the rated and fluctuating power states are decreased by 49.7% and 51.3%, respectively.

To offer a better guidance for the actual renewable energy driven hydrogen production system, it is necessary to carry out comprehensive technical and economic analysis of the hybrid hydrogen generation system under the developed variable-period sequence control strategies.

CRediT authorship contribution statement

Xianyang Liu: Investigation, Visualization, Writing – original draft. **Jun Zou:** Investigation. **Rui Long:** Conceptualization, Methodology, Supervision, Writing – review & editing, Funding acquisition. **Zhichun Liu:** Conceptualization. **Wei Liu:** Conceptualization, Supervision.

Declaration of competing interest

The authors declare that they have no known competing financial interests or personal relationships that could have appeared to influence the work reported in this paper.

Acknowledgments

This work was financially supported by the National Key Research and Development Program of China (2022YFB4003801).

References

[1] E. Bozoglan, A. Midilli, A. Hepbasli, Sustainable assessment of solar hydrogen production techniques, Energy 46 (1) (2012) 85–93.
[2] S. Toghyani, E. Afshari, E. Baniasadi, S.A. Atyabi, Thermal and electrochemical analysis of different flow field patterns in a PEM electrolyzer, Electrochim. Acta 267 (2018) 234–245.
[3] Z. Su, S. Ding, Z. Gan, X. Yang, Analysis of a photovoltaic-electrolyser direct-coupling system with a V-trough concentrator, Energy Convers. Manag. 108 (2016) 400–410.
[4] R.E. Clarke, S. Giddey, F.T. Ciacchi, S.P.S. Badwal, B. Paul, J. Andrews, Direct coupling of an electrolyser to a solar PV system for generating hydrogen, Int. J. Hydrogen Energy 34 (6) (2009) 2531–2542.
[5] Z. Su, S. Ding, Z. Gan, X. Yang, Optimization and sensitivity analysis of a photovoltaic-electrolyser direct-coupling system in Beijing, Int. J. Hydrogen Energy 39 (14) (2014) 7202–7215.
[6] T. Gibson, N. Kelly, Optimization of solar powered hydrogen production using photovoltaic electrolysis devices, Int. J. Hydrogen Energy 33 (21) (2008) 5931–5940.
[7] R. Garciavalverde, C. Miguel, R. Martinezbejar, A. Urbina, Optimized photovoltaic generator–water electrolyser coupling through a controlled DC–DC converter, Int. J. Hydrogen Energy 33 (20) (2008) 5352–5362.
[8] T.L. Gibson, N.A. Kelly, Predicting efficiency of solar powered hydrogen generation using photovoltaic-electrolysis devices, Int. J. Hydrogen Energy 35 (3) (2010) 900–911.
[9] L. Arriaga, W. Martinez, U. Cano, H. Blud, Direct coupling of a solar-hydrogen system in Mexico, Int. J. Hydrogen Energy 32 (13) (2007) 2247–2252.
[10] Z. Liu, Z. Qiu, Y. Luo, Z. Mao, C. Wang, Operation of first solar-hydrogen system in China, Int. J. Hydrogen Energy 35 (7) (2010) 2762–2766.
[11] F. Barbir, PEM electrolysis for production of hydrogen from renewable energy sources, Sol. Energy 78 (5) (2005) 661–669.
[12] N.A. Kelly, T.L. Gibson, D.B. Ouwerkerk, Generation of high-pressure hydrogen for fuel cell electric vehicles using photovoltaic-powered water electrolysis, Int. J. Hydrogen Energy 36 (24) (2011) 15803–15825.
[13] N. Kelly, T. Gibson, D. Ouwerkerk, A solar-powered, high-efficiency hydrogen fueling system using high-pressure electrolysis of water: design and initial results, Int. J. Hydrogen Energy 33 (11) (2008) 2747–2764.
[14] O. Atlam, F. Barbir, D. Bezmalinovic, A method for optimal sizing of an electrolyzer directly connected to a PV module, Int. J. Hydrogen Energy 36 (12) (2011) 7012–7018.
[15] B. Paul, Optimal coupling of PV arrays to PEM electrolysers in solar–hydrogen systems for remote area power supply, Int. J. Hydrogen Energy 33 (2) (2008) 490–498.
[16] A. Maroufmashat, F. Sayedin, S.S. Khavas, An imperialist competitive algorithm approach for multi-objective optimization of direct coupling photovoltaic-electrolyzer systems, Int. J. Hydrogen Energy 39 (33) (2014) 18743–18757.
[17] E. Akyuz, C. Coskun, Z. Oktay, I. Dincer, Hydrogen production probability distributions for a PV-electrolyser system, Int. J. Hydrogen Energy 36 (17) (2011) 11292–11299.
[18] J.M. Vidueira, A. Contreras, T.N. Veziroglu, PV autonomous installation to produce hydrogen via electrolysis, and its use in FC buses, Int. J. Hydrogen Energy 28 (9) (2003) 927–937.
[19] J.O.M. Bockris, T.N. Veziroglu, Estimates of the price of hydrogen as a medium for wind and solar sources, Int. J. Hydrogen Energy 32 (12) (2007) 1605–1610.
[20] E. Bilgen, Domestic hydrogen production using renewable energy, Sol. Energy 77 (1) (2004) 47–55.
[21] A. Brka, Y.M. Al-Abdeli, G. Kothapalli, Predictive power management strategies for stand-alone hydrogen systems: operational impact, Int. J. Hydrogen Energy 41 (16) (2016) 6685–6698.
[22] D. Ipsakis, S. Voutetakis, P. Seferlis, F. Stergiopoulos, C. Elmasides, Power management strategies for a stand-alone power system using renewable energy sources and hydrogen storage, Int. J. Hydrogen Energy 34 (16) (2009) 7081–7095.
[23] K. Zhou, Optimal energy management strategy and system sizing method for stand-alone photovoltaic-hydrogen systems, Int. J. Hydrogen Energy 33 (2) (2008) 477–489.
[24] Ø. Ulleberg, The importance of control strategies in PV–hydrogen systems, Sol. Energy 76 (1–3) (2004) 323–329.
[25] T. Alnejaili, S. Drid, D. Mehdi, L. Chrifi-Alaoui, R. Belarbi, A. Hamdouni, Dynamic control and advanced load management of a stand-alone hybrid renewable power system for remote housing, Energy Convers. Manag. 105 (2015) 377–392.
[26] R. Fang, Y. Liang, Control strategy of electrolyzer in a wind-hydrogen system considering the constraints of switching times, Int. J. Hydrogen Energy 44 (46) (2019) 25104–25111.
[27] F. Valenciaga, C.A. Evangelista, Control design for an autonomous wind based hydrogen production system, Int. J. Hydrogen Energy 35 (11) (2010) 5799–5807.
[28] A. Abdelkafi, L. Krichen, Energy management optimization of a hybrid power production unit based renewable energies, Int. J. Electr. Power Energy Syst. 62 (2014) 1–9.
[29] T. Zhou, B. Francois, Modeling and control design of hydrogen production process for an active hydrogen/wind hybrid power system, Int. J. Hydrogen Energy 34 (1) (2009) 21–30.
[30] J.P. Torreglosa, P. García, L.M. Fernández, F. Jurado, Energy dispatching based on predictive controller of an off-grid wind turbine/photovoltaic/hydrogen/battery hybrid system, Renew. Energy 74 (2015) 326–336.
[31] W. Won, H. Kwon, J.-H. Han, J. Kim, Design and operation of renewable energy sources based hydrogen supply system: technology integration and optimization, Renew. Energy 103 (2017) 226–238.
[32] A.M.O. Haruni, M. Negnevitsky, M.E. Haque, A. Gargoom, A novel operation and control strategy for a standalone hybrid renewable power system, IEEE Trans. Sustain. Energy 4 (2) (2013) 402–413.
[33] Y. Gu, X. Xiang, W. Li, X. He, Mode-adaptive decentralized control for renewable DC microgrid with enhanced reliability and flexibility, IEEE Trans. Power Electron. 29 (9) (2014) 5072–5080.
[34] J. Gabrielgarciaclua, R. Julianmantz, H. Debattista, Hybrid control of a photovoltaic-hydrogen energy system, Int. J. Hydrogen Energy 33 (13) (2008) 3455–3459.
[35] M. Trifkovic, M. Sheikhzadeh, K. Nigim, P. Daoutidis, Modeling and control of a renewable hybrid energy system with hydrogen storage, IEEE Trans. Control Syst. Technol. 22 (1) (2014) 169–179.
[36] K. Ishaque, Z. Salam, H. Taheri, Simple, fast and accurate two-diode model for photovoltaic modules, Sol. Energy Mater. Sol. Cell. 95 (2) (2011) 586–594.
[37] Sera D, Teodorescu R, Rodriguez P. PV panel model based on datasheet values. Conference PV Panel Model Based on Datasheet Values. p. 2392-2396.
[38] R. Long, B. Li, Z. Liu, W. Liu, Performance analysis of a solar-powered electrochemical refrigerator, Chem. Eng. J. 284 (2016) 325–332.
[39] A. Dicks, D. Rand, Fuel Cell Systems Explained, 2018.
[40] K.W. Harrison, E. Hernández-Pacheco, M. Mann, H. Salehfar, Semiempirical model for determining PEM electrolyzer stack characteristics, J. Fuel Cell Sci. Technol. 3 (2) (2005) 220–223.
[41] S. Toghyani, E. Afshari, E. Baniasadi, S.A. Atyabi, G.F. Naterer, Thermal and electrochemical performance assessment of a high temperature PEM electrolyzer, Energy 152 (2018) 237–246.
[42] J.J. Hwang, L.K. Lai, W. Wu, W.R. Chang, Dynamic modeling of a photovoltaic hydrogen fuel cell hybrid system, Int. J. Hydrogen Energy 34 (23) (2009) 9531–9542.
[43] T.E. Springer, T.A. Zawodzinski, S. Gottesfeld, Polymer electrolyte fuel cell model, J. Electrochem. Soc. 138 (8) (1991) 2334.
[44] F. Marangio, M. Santarelli, M. Cali, Theoretical model and experimental analysis of a high pressure PEM water electrolyser for hydrogen production, Int. J. Hydrogen Energy 34 (3) (2009) 1143–1158.
[45] A.Z. Weber, R.L. Borup, R.M. Darling, P.K. Das, T.J. Dursch, W. Gu, et al., A critical review of modeling transport phenomena in polymer-electrolyte fuel cells, J. Electrochem. Soc. 161 (12) (2014) F1254–F1299.
[46] H. Zhu, R.J. Kee, A general mathematical model for analyzing the performance of fuel-cell membrane-electrode assemblies, J. Power Sources 117 (1–2) (2003) 61–74.
[47] E. Hernández-Pacheco, D. Singh, P.N. Hutton, N. Patel, M.D. Mann, A macro-level model for determining the performance characteristics of solid oxide fuel cells, J. Power Sources 138 (1) (2004) 174–186.
[48] L.-Y. Chu, S.-H. Park, T. Yamaguchi, S-i Nakao, Preparation of thermo-responsive core-shell microcapsules with a porous membrane and poly(N-isopropylacrylamide) gates, J. Membr. Sci. 192 (1) (2001) 27–39.

[49] M. Ni, M.K.H. Leung, D.Y.C. Leung, An electrochemical model of a solid oxide steam electrolyzer for hydrogen production, Chem. Eng. Technol. 29 (5) (2006) 636–642.
[50] D. Toumi, D. Benattous, A. Ibrahim, H.I. Abdul-Ghaffar, S. Obukhov, R. Aboelsaud, et al., Optimal design and analysis of DC–DC converter with maximum power controller for stand-alone PV system, Energy Rep. 7 (2021) 4951–4960.
[51] Salam Z, Ishaque K, Taheri H. An improved two-diode photovoltaic (PV) model for PV system. Conference an Improved Two-Diode Photovoltaic (PV) Model for PV System. p. 1-5.
[52] Z. Abdin, C.J. Webb, E.M. Gray, Modelling and simulation of a proton exchange membrane (PEM) electrolyser cell, Int. J. Hydrogen Energy 40 (39) (2015) 13243–13257.